This is a preprint, the final version is subject to change, of the American Mineralogist (MSA)
Cite as Authors (Year) Title. American Mineralogist, in press.
DOI: https://doi.org/10.2138/am-2020-7221

Revision 1

In-situ measurements of magmatic volatile elements, F, S and Cl, by electron microprobe, secondary ion mass spectrometry, and heavy ion elastic recoil detection analysis

Estelle F. Rose-Koga[1], Kenneth T. Koga[1], Jean-Luc Devidal[1], Nobumichi Shimizu[2], Marion Le Voyer[3], Celia Dalou[4], Max Döbeli[5].

(1) Université Clermont Auvergne, CNRS UMR6524, IRD, OPGC, Laboratoire Magmas et Volcans, F-63000 Clermont-Ferrand, France

(2) Woods Hole Oceanographic Institution, Dpt Geology & Geophysics, MA, USA

(3) Smithsonian Institution, National Museum of Natural History, PO Box 37012, MRC 119, Washington, DC 20013, USA

(4) Centre de Recherches Pétrographiques et Géochimiques, UMR7358, CNRS - Université de Lorraine, BP20, 54501 Vandoeuvre-lès-Nancy Cedex, France

(5) Laboratory for Ion Beam Physics, ETH Zürich, Zürich, Switzerland

Abstract

The electron probe (EPMA) and ion probe (SIMS) are the two most used instrument for *in situ* analysis of halogens in geological materials. The comparison of these two methods on widely distributed glass standards (ex: MPI-DING) illustrates the performance of each methods for measuring volatile elements and establishes concrete thresholds for choosing one over the other (e.g. detection limit, precision, accuracy and

matrix effect). We report analyses of F, S and Cl concentrations in 3 geological glass samples (EPMA) and 10 reference standards (EPMA and SIMS). Furthermore, F and Cl absolute abundances have been determined independently for three of the standards (KL2-G, ATHO-G and KE12) via heavy ion elastic recoil detection analysis (HIERDA), to certify the accuracy of the cross-calibration of EPMA and SIMS. The detection limits for EPMA are a 150 $\mu g.g^{-1}$ for F, 30 $\mu g.g^{-1}$ for S and 20 $\mu g.g^{-1}$ for Cl and for SIMS < 48 $\mu g.g^{-1}$ for F, < 3 $\mu g.g^{-1}$ for S and <19 $\mu g.g^{-1}$ for Cl. On SiO_2-rich glass-standards, F and Cl measurements by HIERDA highlight a weak matrix effect during SIMS analysis of F and Cl. With the HIERDA independently measured value, we therefore propose an alternative calibration function to empirically correct this matrix effect on the SIMS measurements of F and Cl and inferred the same method for the alternative calibration of S.

Keywords: F, Cl, SIMS, EPMA, ERDA, melt inclusion

Introduction

The behavior of trace volatile elements (magmatic volatile components other than H_2O and CO_2) in magmas has inspired many scientific contributions in the past decades (e.g. Baker et al., 2005; Wallace, 2005; Behrens and Gaillard, 2006; Fischer, 2008; Aiuppa et al., 2009 and reference therein). There are several extensive reviews of the interest of halogens in Earth Sciences (Aiuppa et al., 2009; Harlov and Aranovich, 2018; Hanley and Koga, 2018). Quantification of volatile element recycling implies the knowledge of the magma volatile element composition prior to degassing. While lavas

erupting from arc volcanoes are at least partially degassed, olivine hosted-melt inclusions found in these lavas, are expected to be less affected by degassing because they are shielded, by the host mineral, from interaction with their surrounding in the magma chamber and during magma ascent. While the shielding does not hold for H_2O, it is true for halogens such as Cl and F. At the pressure and temperature conditions of melt inclusion formation, (1) they are less prone to degassing (if at all) than H_2O (e.g. Carroll and Webster, 1994; Métrich and Wallace, 2008), and (2) F and Cl do not diffuse significantly through the host-olivine (e.g., Gaetani et al., 2012; Bucholz et al. 2013; Lloyd et al. 2013; Le Voyer et al. 2014). Halogen measurements in arc melt inclusions have proven to retain the information of magma genesis (Koga *et al.* 2009; Bucholz et al., 2013; Rose-Koga et al., 2012, 2014) along with other lithophile trace elements (such as REE; e.g. Cabral et al., 2014; Jackson et al., 2015; Rose-Koga et al., 2017; Narvaez et al., 2018). The subduction input/output mass balance calculations show that nearly 100% of Cl entering subduction zone is incorporated in arc magmatism, compared to only about 50% of F (e.g. Straub and Layne 2003; Wallace 2005). Therefore Cl and F are ideal tracers to identify the fractionation process between the slab and the flux originating from it, especially since they are scarcely present in the mantle (F reservoirs, see for example Koga and Rose-Koga, 2014; 2018). Moreover, recent experimental results have determined F and Cl partition coefficients between melt and crystals (e.g. Dalou et al., 2014) and put forward that the large variation of F/Cl in arc melt inclusions resulted from the composition, the amount of slab contribution to the magma and the degree of melting (e.g. Narvaez et al., 2018).

Here we compare *in situ* analytical technics for F and Cl measurements because the smaller and smaller geological samples, today, that we are studying are requiring intercalibration and comparison of analytical techniques to make educated decisions on which one to use to achieve the goals we set. With recent advances of micro analytical techniques and melt inclusion studies, there is a growing body of concentration measurements of relatively volatile, light-atomic-mass elements (H, B, C, F, S, Cl) in MORB glasses and primitive melts of subduction zone magmas (*e.g.* with SIMS: Sisson and Layne 1993; Métrich *et al.* 1999; Hauri et al., 2002; Wade *et al.* 2006; Le Voyer *et al.* 2008, 2010; Bouvier et al., 2008; 2010; Rose-Koga *et al.* 2012; 2014; see also references in Wallace 2005 and with NanoSIMS *e.g.* Bartoli et al., 2014; Créon et al., 2017, 2018; Carvalho et al., 2019). Other volatile elements, moderatly heavier, such as Br, have also been successfully measured by secondary ion mass spectrometry (Cadoux et al., 2017).

Among the difficulties contributing to the limited comparison of the pre-existing data, was, suprisingly, the lack of published comparisons of S, Cl and F measurements of standards between the two most used *in situ* analytical procedures: the electron microprobe (EPMA) and the ion probe (SIMS). While recent precise rock and glass analysis exist (e.g.: Shimizu et al., 205; 2017), *in situ* methods to measure halogens are rarely compared. Recently, a F, S and Cl comparison between literature data obtained by EPMA and by SIMS (Le Voyer et al., 2019) concluded that inter-laboratory comparisons agreed within 10% for F and to a variable degree for S and Cl, and proposed a quality controlled published-data summary table (Table S2 available through the EarthChem Library, http://dx.doi.org/10.1594/IEDA/111195). Electron microprobes perform

microanalysis of volatile elements, but the high detection limits of this technique (tens to hundreds of ppm) place limitations on many volatile studies (cf. Devine *et al.* 1995 and references therein).

In this paper we measure F, S and, Cl by SIMS on a set of 6 glasses from the WHOI standard-set (ALV519-4-1, ALV1654-3, ALV1649-3, GL03-D51-3, GL07-D52-5, EN113-46D-2) to create 3 working curves. We use our 3 SIMS working curves to compare our SIMS measured values of 8 MPI DING glasses (ML3B-G, KL2-G, StHs6/80-G, GOR128-G, GOR132-G, ATHO-G, T1-G, KE12) and of 2 basaltic standards (VG2 and VG-A99) with our EPMA values. We also report independent, absolute F and Cl values from elastic recoil detection analysis (HIERDA) of three MPI DING glasses (KE12, ATHO-G and KL2G) which independently anchors our calibration curves.

Standards and glass samples

All glasses and standards used have already been well documented elsewhere, and we summarize here the essential points. The set of 6 basalt samples used in this study for the SIMS analysis come from several sources (Table 1). The ALV standards are fresh basaltic glasses sampled during Alvin dives over the Famous area (ALV519-4-1: Shimizu 1998; Michael and Cornell 1998), and over the Galapagos Spreading Center 85ºW (ALV1654-3 and ALV1649-3; Embley *et al.* 1988; Perfit *et al.* 1998). GL standards are fresh basalt glasses from the Salas y Gomez seamount area (GL03-D51-3 and GL07-D52-5; Simons *et al.* 2002). EN113-46D-2 is a fresh basaltic glass from the Endeavor spreading center (Simons *et al.* 2002).

For the other glass samples and standards we used six basalts (KL2-G, a glass from Kilauea volcano, Hawaii; ML3B-G from Mauna Loa Volcano, Hawaii; VG2, *aka* USNM 111240/52, a glass from the Juan de Fuca Ridge (Jarosewich 2002); VG-A99, aka A99, USNM 113498/1, a glass from Kilauea volcano, Hawaii (Jarosewich *et al.* 1979); Alvin 2746-15, a glass from 9-10ºN East Pacific Rise (Bowles *et al.* 2006); Alvin 2390-5, a glass from the Siqueiros Transform, (Sims *et al.* 2002)), one andesitic glass, (StHs6/80-G, Mt. St. Helens, USA, Jochum *et al.* 2000), two komatiitic glasses, (GOR128-G and GOR132-G both from Gorgona Island, Jochum *et al.* 2000), a rhyolitic glass, (ATHO-G, from Iceland, Jochum *et al.* 2000), a quartz-diorite glass, (T1-G, from the Italian Alps, Jochum *et al.* 2000), two obsidians, (Sletta, from Iceland, courtesy from O. Sigmarsson; and KE12 from Eburru, Kenya; personnal communication of Malik and Bungard, personal communication in 1974, cited in Devine *et al.* 1984).

Analytical procedures

EPMA analysis

Electron microprobe analyses were performed with a Cameca SX 100 equipped with four wavelength dispersive spectrometers (WDS) at the Laboratoire Magmas et Volcans (Clermont-Ferrand). Major elements and volatiles were analyzed in separate analytical sessions with the following detailed conditions. Major elements in glasses were analyzed at an accelerating voltage of 15 kV, an 8 nA beam current and a 20 µm defocused beam. These analytical conditions are well suited for glasses analyses; no geochemical instability (sodium loss principally) is detected even for silica rich samples (e.g. Oladottir *et al.* 2011).

Chlorine, sulfur and fluorine analyses were performed at 80 nA and with a 5 to 20 µm defocused beam together with the trace element acquisition program in the Cameca Peak Sight software. This quantification model takes into account the matrix composition of the glass to calculate the traces element concentration. ZAF data reduction was carried out by the means of the X-PHI model. The analytical standards were: natural scapolite for the Cl$K\alpha$ line, fluorite for F$K\alpha$ and VG-2 glass for S$K\alpha$. Sulfur concentration in VG-2 glass is 1340 $\mu g.g^{-1}$; this value corresponds to the average of a compilation of published data (Dixon *et al.* 1991; Thordarsson *et al.* 1996; Thornber *et al.* 2002). Counting times are discussed in detail below.

Sulfur and chlorine. Because sulfur speciation (S^{6+} or S^{2-}) induces changes in the S$K\alpha$ spectral position (Carroll and Rutherford 1988), prior to sulfur concentration measurement and for every sample, the S$K\alpha$ peak maximum was first located by using the automated peak-scan routine of the Cameca SX 100 software. Then, if the measured peak position differs from the one of the standard, the new value is recorded in the analysis setup. The selection of the diffraction crystals is decided by the achievements of the highest peak counts to reach very low detection limits and by looking at the region of the spectrum with no interfering peaks. Thus, chlorine and sulfur were analyzed successively by using a large pentaerythritol (LPET) crystal.

Fluorine. The case of fluorine is more complex. This element can be measured either with a W/Si multilayer crystal (PC1) or with a thallium acid phthalate crystal (TAP). The multilayer crystal allows high precision and accuracy measurements together with low detection limits. Unfortunately, for iron-bearing minerals or glasses, the F$K\alpha$

peak is strongly overlapped by the shoulder of a strong Fe$L\alpha$ line. Different studies (Todd 1996; Witter and Kuehner 2004; Zhang et al. 2016) have proposed an electron microprobe method for analyzing F in Fe-bearing minerals and glasses using multilayer crystals that overcomes the spectral interference. This method is based on the linear relationship existing between the iron concentration of fluorine-free minerals (olivine and pyroxenes essentially) and the number of counts at the F$K\alpha$ peak position in the same fluorine-free minerals. Thus, the Fe$L\alpha$ contribution (i.e. the background) can be easily deduced and quantified from the total iron concentration of the sample and subtracted from the bulk F*Ka* peak counts. However, the calibration curve of this model is only found for the analysis of Fe^{2+}-bearing minerals. In transition metals of the first row, the L-spectra exhibit peak position shifts as a function of the oxidation state (Fialin *et al.* 2001, 2004). The omission of the self-absorption induced shift of the $L\alpha$ peak between Fe^{2+} and Fe^{3+} could lead to the overestimation of the background counts at F*Ka* peak position and thus to an underestimation of the fluorine content. The correction method established by Witter and Kuehner (2004) should be only applied for pure Fe^{2+}-bearing minerals and glasses. In order to overcome this problem, we analyzed fluorine using TAP diffraction crystals although the detector is significantly less efficient than PC1. To improve its counting statistics (precision and detection limit), fluorine was measured simultaneously on 3 spectrometers according to the Cameca multi-spectrometers counting routine. On top of the choice of the detector, we tested CaF_2 and Durango apatite standards for F calibration, and concluded that CaF_2 provides generally consistent results, most likely due to known F X-ray excitation issue of apatite (Stormer et al., 1993).

The challenge with trace element analysis in glass is to find a compromise between low detection limit, *i.e.* the use of high beam current, long counting time, and limited beam damages. Volatile loss during the analysis is minimized through the used of a protocol derived from the CSIRO-trace routine (Robinson and Graham 1992). The total counting time (peak and background) for a single analysis is 40 sec and is divided as follow: 10 sec on peak and background for chlorine and sulfur but 60 sec on peak and background for fluorine (20 sec per spectrometer). A low detection limit is achieved by increasing the number of analyses on the same point, thus improving the signal-to-noise ratio. After each analysis, the beam is shielded for 20 sec allowing the sample to cool down. Total volatile concentrations are calculated from the sum of the counts from the successive iterations. With 15 kV accelerating voltage and 80 nA beam current, for a total Cl and S peak counting time of 100 sec and 600 sec for F. Typical detection limits for F, Cl, and S were 150, 20 and 30 $\mu g.g^{-1}$, respectively. The analytical volume ranges from the order of 10^2 to 10^3 μm^3.

SIMS analysis

Sample preparation for SIMS. The standards are mounted in high purity indium metal (e.g. Hauri *et al.* 2002; Le Voyer *et al.* 2008) in a 1 inch diameter aluminum ring, washed in an ultrasonic bath with pure ethanol then with distilled water for 10 minutes each time. Indium is used because epoxy contains significant amounts of volatile molecules that can degass during the analysis, deteriorate the quality of vacuum, and increase the background signal. The mount is dried carefully in an oven overnight. The mount is finally gold coated before analysis and kept overnight in high vacuum (low 10^{-8} torrs) until being introduced in the sample chamber.

Method. The measurements for the working curve calibrations were done on a set of 6 glass standards (Table 1), on the Cameca 1280 ion probe of Woods Hole Oceanographic Institution (MA, USA). We used a Kohler illumination with a primary beam current of 1.5 nA Cs^+ primary positive beam, and negatively charged secondary ions were extracted through a nominal accelerating potential of 10 kV. Due to implantation of Cs^+ ions and extraction of both negatively charged secondary ions and electrons, positive charging of the sample surface must be compensated with the use of an electron flood gun which delivers electrons to the sample surface. The isobaric interferences were filtered by an energy slit opening at 50 eV and the contrast aperture at the cross over was large (400 µm). The entrance and exit slits were closed to achieve a mass resolution of $M/\Delta M=5800$. With this resolution, the interfering signals were effectively separated for F, S, and Cl (Fig. 1).

We presputtered the sample surfaces during 180 seconds while applying a raster of 30×30 µm. The field aperture (of 8000), which corresponds to an area of 15×15 µm, is inserted into the image plane. This means that only the ions originating from the central 15 µm square of the flat-bottomed sputtered-crater are admitted into the mass spectrometer. The elimination of stray ions sputtered from the crater walls and desorbed from the sample surface results in very low volatile backgrounds (routinely about 0.05–0.1 counts per second for the counting system at half mass positions with the primary beam and the electron gun on). We counted 8 sec on ^{19}F, 5 sec on ^{30}Si, 5 sec on ^{32}S and 8 sec on ^{35}Cl. One analysis was composed of 2 blocks of 10 cycles and took less than 15 min per spot. Intensities of ^{19}F, ^{32}S and ^{35}Cl were collected cyclically by an electron

multiplier, processed through pulse-counting electronics and normalized to ^{30}Si for concentration calculations.

Calibration. Earlier studies that have involved Cs^+ beam were performed on a small format SIMS (Cameca 6f, Hauri *et al.* 2002). However, hydride interferences, such as SH^-, are difficult to effectively eliminate using the energy filtering technique (Shimizu *et al.* 1978) available on small format Cameca instruments (e.g., IMS 3f/4f/5f/6f/7f). The high mass resolution of the SIMS 1280 model is required to eliminate the $^{34}S^1H$ interference on ^{35}Cl (MRP>5120) without giving up transmission significantly (Fig. 1c). The SIMS calibration curves for F, S and Cl are shown in Fig. 2. They are regressions of ion probe signals (x-axis) compared to known EPMA concentrations (y-axis). The former is the intensity ratio of two elements times the SiO_2 concentrations of each standards, the numerator of the ratio being the element of interest and the denominator is a matrix element common to all samples (*e.g.* $^{19}F/^{30}Si$). Typically, here ^{19}F, ^{32}S and ^{37}Cl are normalized against ^{30}Si. This provides a robust analysis little influenced by primary beam fluctuations or by ionization efficiency changes owing to matrix effects (Shimizu and Hart, 1982). In fact, the calibrations for F, S and Cl are free of significant matrix effects. The calibration curve is determined at the beginning and at the end of each session to assure no significant drift has taken place.

Detection limit. With the calibration curves of the standards, we attributed the Y-intercept of the linear regression to the detection limit (*e.g.* Ihinger *et al.* 1994). We stress that this method is not accurate enough and depends on the uncertainties of the regressed data, and the leverage of the data for the higher concentrations being potentially unreasonable. Ideally, only the measurements of standards with F, S, and Cl

concentrations lower than the expected background can give the detection limit (see Koga et al., 2003, for this procedure during low hydrogen concentration measurements by SIMS). It was not a simple task to verify sub-ppm-level abundance, and we are not aware of any micro analytical method that can independently verify sub-ppm-level abundance of these elements. It should be noted that for the abundance of H_2O, FTIR analyses were used for the blank verification. Therefore, we adapted the calibration without explicitly identifying zero-point count rate as this method is less prone to inter-laboratory biases (Table 1). Some studies have used adapted "blank" material such as San Carlos olivine, synthetic forsterite, and high-purity quartz glass (Hauri et al. 2002, Le Voyer et al. 2017, Shimizu et al. 2017). With what was available to us we calculated detection limits 48 $\mu g.g^{-1}$ for F, 3 $\mu g.g^{-1}$ for S and 19 $\mu g.g^{-1}$ for Cl (Fig. 2). These values are effectively the zero intercept within the regression uncertainties. In addition, the linear regression of the calibration curve is equivalent to forcing the regression through zero. The slopes between forcing the linear regression through zero (red curve Fig. 2) and classic linear regression with a non-zero intercept (blue curve Fig. 2) is identical within error.

A detection limit of <1 $\mu g.g^{-1}$ for F, S, and Cl was previously reported with a 6f ion probe (Hauri *et al.* 2002; <2 $\mu g.g^{-1}$ for F; Guggino and Hervig 2010). With a 1280 ion probe detection limits down to 0.2 $\mu g.g^{-1}$ for S and Cl, and 0.1 $\mu g.g^{-1}$ for F can be achieved with "blank" standards (Le Voyer et al., 2019). Our analytical standard error (σ over the 20 cycles) was typically 0.6 % for F, S and Cl (compared to 1% in Le Voyer et al., 2019) and the reproducibility on the standards (2RSD) was 6.3, 3.5 and 5.2%, respectively (n=14, ALV519-4-1; comparable to 5.8, 7.6 and 10.8%, respectively, on in-run standard glass P1326-2, Helo et al., 2011; 7, 4 and 7%, respectively on glass VG2, Le

Voyer et al., 2019). This is compared to the long-term external reproducibility (2 RSD) of standard ALV519-4-1 by EPMA was 55.3, 5.2 and 58.3%, for F, S and Cl, respectively. The analytical volume is on the order of 10^2 μm^3.

Elastic Recoil Detection Analysis (ERDA)

ERDA is an absolute measurement independent from the two previous methods (EPMA and SIMS). The method is absolute because it consists of a collision between the nuclei of 2 atoms and the radii of the two nuclei (*i.e.* collision cross-section, for example ^{19}F and ^{127}I) are known with great precision, and therefore the ERDA method determines accurate statisical distributions of atoms in a substrate. Therefore, with a known oxygen abundance, fluorine concentration is calculated from a F/O ratio. ERDA has previously been used to measure hydrogen in geological materials (*e.g.* Mosbah et al., 1990; Bureau et al., 2009) or to intercalibrate with infrared spectroscopy measurements (e.g. Aubaud et al., 2009; Withers et al., 2012). The ERDA were conducted at ETH Zurich, in the Ion Beam Physics laboratory of the Paul Scherrer Institut. We used a primary ion beam of Heavy Ion ^{127}I at 12 MeV, therefore the method is specifically called HIERDA (Döbeli et al., 2005). This iodine beam was produced by EN-tandem accelerator via cesium (Cs) sputtering of AgI. For lower projectile energies Time of Flight-ERDA (ToF-ERDA) is a widely used technique. The analytical protocol is only briefly explained in the following, full details can be found in C. Kottler *et al.* 2006 (and reference therein). The beam hits the polished plane of the sample with a low angle and the scattered element of choice (F and Cl, here) are detected by the ToF-ERDA dectector at the fixed angle of 36º. The recoil masses are identified by means of a coincident measurement of the particle velocity and total energy. The recoil energy for ^{19}F is 3.5 MeV and that of ^{35}Cl is 5.3 MeV. Here a

gas ionization chamber (GIC) instead of silicon detectors has been used for energy measurements because silicon detectors suffer from considerable radiation damage. This detector assured a resolution of energy spectra better than 1 MeV, allowing the precise separation of different atoms. The mass resolving power is $M/\Delta M = 40$ for the mass range corresponding to F and Cl. The shape of the beam on the sample is a rectangle of 1 mm × 4 mm but only a small part of it was actually targeting the sample, the rest was hitting the surrounding indium. A classical ERDA graph displays a time of flight curve for each ion versus energy (Kottler *et al.* 2006). These curves are processed to extract a spectrum for each elements (Fig. 3a, b, c). The detection limits were derived from off-peak baseline noise level. The entire glass chip was bombarded by ^{127}I beam and the accessible depth at this energy is approximately 200 nm (Dobeli et al., 2005). The analytical volume is on the order of 10^5 μm^3.

Results

There is a good general agreement on mafic standards for the measurements of F, S and Cl between EPMA and SIMS above a certain threshold of concentrations, >150 $\mu g.g^{-1}$ for F, and >30 $\mu g.g^{-1}$ for S and >20 $\mu g.g^{-1}$ for Cl (Fig. 4). For F<150 $\mu g.g^{-1}$ SIMS can measure differences in F concentrations with a precision better than 10% relative when EPMA has a precision equal to the measured value (Fig. 4a). The performance of both EPMA and SIMS are in excellent agreement for Cl measurements down to 20 $\mu g.g^{-1}$ (Fig. 4c). But for S measurements, SIMS can measure S concentrations below 10 $\mu g.g^{-1}$ when EPMA will not measure resolvable difference in standards with S<10 $\mu g.g^{-1}$ (Fig. 4b).

The glass standards measured here have reported values that can vary up to a factor of 10 for certain elements (*e.g.* Cl in StHs6/80; Table 2). Nonetheless, overall we note that technical improvements of in-situ instruments make it possible to reach interlaboratory agreements. Our EPMA and SIMS measurements mostly agree within error with the reported values published since 2006 (*e.g.* Jochum et al., 2006), simply improving the precision in some cases. When they do not agree, we can invoke millimeter scale heterogeneity of the standards. They have been reported for trace elements in the ATHO-G rhyolite (MPI-DING; Borisova et al., 2010) and caution must be applied when choosing the standards to perform micro-analysis. For example it is clear from Table 2 that our ATHO-G piece is very different than the piece measured by SIMS in Jochum et al, 2006, and closer to the composition of that of Oskarsson et al. (1982). In any case, this disparity has nothing to do with the quality of the analysis. In this respect, ATHO-G and StHs6/80-G appears to be heterogenous for F, S and Cl depending on the individual pieces that maybe available in different labs. Also, the 2σ error we report for our EPMA are, 9 times out of 10, better than previously reported, demonstrating that the proposed settings for halogen measurements by EPMA are particularly well suited for halogen analysis.

The ERDA results for F and Cl in ATHO-G, KE12 and KL2-G anchors independently the calibration curves for F and Cl. We note that the ERDA values for F and Cl of the two SiO_2-rich standards, are closer to the EPMA values than the SIMS values (Fig. 4a and 4c), and the ERDA measurement on the basalt standard KL2-G was difficult to assess because of the high detection limit of the ERDA.

Discussion

Precision and accuracy

The lowest concentrations we measured were samples GOR-128 and GOR-132 for F and S and sample StHs for Cl (Table 2). While EPMA measurements tend to level out around 10 $\mu g.g^{-1}$ concentration for S (Fig. 4b), SIMS measurements are precise to $\mu g.g^{-1}$ level for S and Cl (Fig.4b and c). For F, S and Cl, SIMS measurements always display smaller error bars (Fig. 4a, b, c) primary due to higher counting statistics. Samples with concentration in S or Cl > 100 $\mu g.g^{-1}$ are analyzed with similar precision by both methods. Measurement of F remains up to 5 times more precise with SIMS than EPMA on the basis of analytical precision determined by counting statistics and for F concentrations above 100 $\mu g.g^{-1}$. Because many standard values are still tied to EPMA measured samples, it appears that the uncertainty of the slope and intercept (Fig. 2) contributes to a final uncertainty similar to EPMA values (Table 2). Therefore, it is strongly recommended to use SIMS when the interest of measurement is to detect variations of concentration among similar samples with a high precision, while EPMA can certainly provide a rapid, good assessment of trace volatile abundances above a certain threshold (150, 30 and 20 $\mu g.g^{-1}$ for F, S and Cl, respectively).

Matrix effect

It is particularly notable that some measured values by SIMS (reported for ATHO-G and KE12; Table 2) significantly differ from those of EPMA and ERDA. Fig. 4 also shows that higher SiO_2 glasses (*e.g.* ATHO and KE12) plot on the right side of the 1:1 line, indicating SIMS measurements are higher than EPMA and ERDA. While such

offset is not present for mafic glasses, which have similar SiO_2 contents as the calibration standards. This offset is present for measurements of F, S and Cl. This systematic disparity related to the composition of material analyzed is called the matrix effect, in which the secondary ion emission is influenced by change either structural or compositional variation of the matrix (e.g. Hauri et al, 2002; Ottolini et al., 2002).

The relative sensitivity factor (RSF) describes the bias of an elemental ratio introduced by SIMS: RSF = $(C_i/C_{ref})\times(I_{ref}/I_i)$, where C_i and C_{ref} are the known atomic concentration of mass i and mass ref, respectively and I denotes the measured signal intensity. Essentially, the slope of the calibration function is a representative RSF of several calibration standards. In fact, RSF cannot distinguish bias of the signal of interest (*e.g.* I_F, I_S, and I_{Cl}) from the signal of reference (I_{Si}). Therefore, the variation of RSF with respect to the composition corresponds to the so-called "matrix effect". Fig. 5 shows the value of RSF calculated for the samples of Fig. 4 as a function of SiO_2, excluding the EPMA data below detection limit. It appears that RSF is slightly negatively correlated against SiO_2, consistent with a presence of matrix effect for the high SiO_2 samples. However, considering the scatter of RSF values, the apparent negative correlation has only a slight statistical significance. Unfortunately, the data acquired here are insufficient to discern the exact role of the "matrix effect". Because of such tendency, van den Bleeken and Koga (2015) concluded from a similar analysis that as a first order, one should be able to determine the abundance of these elements without significant correction. A similar conclusion is also reached, via SIMS volatile element measurements of rhyolitic glass with basaltic calibration standards (Shimizu et al. 2017). While this has nothing to do with F and Cl analysis, it has been shown for hydrogen measurements by

SIMS that H^+ emission correlates with the molar mass of the substrate, suggesting that the matrix effect can be effectively corrected with matrix compositions (King et al. 2002). According to their calibration, there is a 40% relative change of H^+ emission coefficient between a basalt and a rhyolite. With the data available today, we did not detect such significant matrix effects for F, S, and Cl comparable to that for H^+. Thus, the variation due to matrix-dependent emissions is expected to be small, and further investigations are certainly needed to identify the exact nature the matrix effect.

Choices of calibration method

Reference mass. Analysis by SIMS requires a ratio of the element of interest (F, S, Cl here) over an element that constitutes the matrix. For silicate glasses, Si is commonly chosen (Shimizu and Hart, 1982). Specifically, ^{30}Si is commonly selected for its low abundance permitting the use of electron multiplier detector. However, depending on the SIMS facility, different reference masses are used. For example, ^{28}Si detected with Faraday cup can be used as the reference mass, as well as $^{18}O^-$ or $^{16}O^-$ providing stable, and high count rate. In general, emission of negative oxygen atom is approximately 10 times better than Si, but this does not to result in a significantly more stable signal. While it will require further study to assess the advantages and disadvantages regarding the choices of the reference mass, a comparison of results from different SIMS labs concluded that it would not influence the measurement significantly (in the electronic supplement, van den Bleeken and Koga, 2015).

Calibration curves. A linear function that converts a SIMS intensity ratio to a concentration can be expressed in following two ways:

$$C_{F,S,Cl} = \alpha \times \left(I_{F,S,Cl}/I_{Si}\right) \times [\mathrm{SiO_2}] + \beta \quad \text{(Eq. 1)},$$

$$C_{F,S,Cl} = \alpha \times \left(I_{F,S,Cl}/I_{Si}\right) + \beta \quad \text{(Eq. 2)}.$$

where, C_i indicates the concentration of an element i, brackets indicates concentration and I_x indicates SIMS intensity (i.e. count rate) of mass x. Slope and Intercept of a regression correspond to α, and β, respectively, which are constants determined by fitting the linear function using known concentration standards. Among SIMS measurements reported, these two equations were commonly used. Equation 2 is sufficient for the measurement with a good match of sample and standard matrices (*i.e.* similar SiO_2 content). In the current study, we adapted Eq. 1, which corrects for variable SiO_2 content (*e.g.* 50% basalt and 70% rhyolite), and produced acceptable results. However, we underline that the Eq. 1 does not correct for the matrix effect discussed above.

It should be noted that if standards and samples have identical SiO_2 then equations 1 and 2 yield identical results. Equation 1 may be considered applicable to a wider range of compositions as it can adjust for the abundance of SiO_2. On the contrary, if oxygen is used as referencing mass instead of Si, as oxygen concentration in silicate varies much less than SiO_2, Equation 1 is unnecessary.

Alternative calibration curves. Recognizing the potential weak correlations between SiO_2 and RSF (Fig. 5), we explored a potential modification of the working curve function with the aim of optimizing the accommodation of SiO_2 variation in silicate glass. With an independent verification of the accuracy by ERDA for high silica samples, the new fitting procedure can be tested without the uncertainty of high concentration

measurements. Furthermore, the revised fitting function should not introduce a bias, if the true working curve is indeed linear. It is an attempt to empirically incorporate a simple matrix effect without changing what we have been doing so far.

In following discussion, we take Cl as an example, and derive the equations. From the definition of RSF, Eq. 1 can be rearranged to show the relationship with RSF.

$$\frac{(C_{Cl}-\beta)}{[\mathrm{SiO_2}]} \times k = \mathrm{RSF} \times \left(\frac{I_{Cl}}{I_{Si}}\right) \qquad \text{(Eq. 1')}.$$

Where k is a conversion factor for a concentration ratio to an atomic ratio, therefore α = RSF/k. Inspecting Fig. 5, we decided to explore two functional forms relating RSF and SiO_2.

$$\mathrm{RSF} = a/[\mathrm{SiO_2}] + b \qquad \text{(Eq. 3)}.$$

$$\mathrm{RSF} = c \times [\mathrm{SiO_2}] + b \qquad \text{(Eq. 4)}.$$

Substituting Eq. 3 or Eq. 4 into Eq. 1', the working calibration curve will be in the following form:

$$C_{Cl} = ak\left(\frac{I_{Cl}}{I_{Si}}\right) + bk\left(\frac{I_{Cl}}{I_{Si}}\right)[\mathrm{SiO_2}] + \beta \qquad \text{(Eq. 5)},$$

$$C_{Cl} = dk\left(\frac{I_{Cl}}{I_{Si}}\right)[\mathrm{SiO_2}] + ck\left(\frac{I_{Cl}}{I_{Si}}\right)[\mathrm{SiO_2}]^2 + \beta \qquad \text{(Eq. 6)}.$$

Table 3 shows the result of the regression with the above two equations. For the regression, in addition to six basaltic calibration standards, three high Si samples are added T1G, ATHO, and KE12. Inspecting the results of the regression, Eq. 6 consistently

produced a better fit, although only slightly, than Eq. 5. On top of this, '*ck*' term is significantly smaller than '*dk*' term in Eq. 6. This suggest that the role of the additional term in correcting the matrix-dependent calibration is minor. This conclusion is again consistent with the discussion above and that of van den Bleeken and Koga (2015) in which authors concluded the use of Eq. 1 is sufficient to determine trace halogen concentration in a wide range of silicate glasses.

While it remains a matter of debate whether to systematically adapt Eq. 6 for the SIMS calibrations, we stress that Eq. 6 is coherent with commonly used calibration curves (Eq. 1 and 2). Another way of proving this is if RSF is constant, (independent of SiO_2 content) then the coefficient c (in Eq. 4) is equal to zero, and this leads to the term with $[SiO_2]^2$ equal to zero in Eq. 6. Therefore Eq. 6 becomes identical to Eq. 1 (with dk = α). For this reason, we think the new calibration function (Eq. 6) is a convenient formulation to be applied to a wide range of SiO_2 glass compositions. In reflection of this spirit, we report concentration values using Eq. 6 in Table 2, indicated as SIMS [Eq. 6].

Implications

An intercalibration of F, Cl and S measurements between EPMA and SIMS is reported for 10 glass-standards, some of them easily accessible to the scientific community (MPI-DING, Jochum et al., 2006). Both analytical methods are in excellent agreement for standards with concentrations in these volatiles elements above 150 $\mu g.g^{-1}$ for F and above 30 $\mu g.g^{-1}$ for S and 20 $\mu g.g^{-1}$ for Cl. However, SIMS has a lower detection limit and is preferable in the case of low concentration samples. The HIERDA measurements independently confirms and anchors our data. This study revealed a shift

between acidic and mafic glass-standard on our HIERDA data, thus requiring (1) cautiousness in the choice of standard materials, and (2) separate SIMS calibrations with standards covering the SiO_2 range of the samples. An alternative is to use the equation 6 that we propose to account for this matrix effect on the SIMS measurements of F, S and Cl.

Acknowledgement: EFR-K thanks O. Sigmarsson for the Sletta sample. EFR-K and KTK acknowledge support from Region Auvergne Rhone Alpes (SCUSI program). This is Laboratory of Excellence *ClerVolc* contribution number 386.

References

Aiuppa, A., Baker, D.R., and Webster, J.D. (2009) Halogens in volcanic systems. Chemical Geology, 263, 1–18.

Aubaud, C., Bureau, H., Raepsaet, C., Khodja, H., Withers, A.C., Hirschmann, M.M., and Bell, D.R. (2009) Calibration of the infrared molar absorption coefficients for H in olivine, clinopyroxene and rhyolitic glass by elastic recoil detection analysis. Chemical Geology, 262, 78–86.

Baker, D.R., Freda, C., Brooker, R.A., and Scarlato, P. (2005) Volatile diffusion in silicate melts and its effects on melt inclusions. Annals of Geophysics, 48, 699-717.

Bartoli, O., Cesare, B., Remusat, L., Acosta-Vigil, A., Poli, S. (2014) The H_2O content of granite embryos. Earth and Planetary Science Letters, 395, 281-290.

Behrens, H., and Gaillard, F. (2006) Geochemical aspects of melts: volatiles and redox behavior. Elements, 2, 275–280.

Borisova, A.Y., Freydier, R., Polvé, M., Jochum, K.P., and Candaudap, F. (2010) Multi-Elemental Analysis of ATHO-G Rhyolitic Glass (MPI-DING Reference Material) by Femtosecond and Nanosecond LA-ICP-MS: Evidence for Significant Heterogeneity of B, V, Zn, Mo, Sn, Sb, Cs, W, Pt and Pb at the Millimetre Scale. Geostandards and Geoanalytical Research, 34, 245–255.

Bouvier, A.S., Métrich, N., and Deloule, E. (2008) Slab-Derived Fluids in the Magma Sources of St. Vincent (Lesser Antilles Arc): Volatile and Light Element Imprints. Journal of Petrology, 49, 1427–1448.

Bouvier, A.-S., Deloule, E., and Métrich, N. (2010) Fluid Inputs to Magma Sources of St. Vincent and Grenada (Lesser Antilles): New Insights from Trace Elements in Olivine-hosted Melt Inclusions. Journal of Petrology, 51, 1597–1615.

Bowles J., Gee J.S., Kent D.V., Perfit M.R., Soule S.A. and Fornari D.J. (2006) Paleointensity applications to timing and extent of eruptive activity, 9º– 10ºN East Pacific Rise. Geochemistry Geophysics Geosystems, 7, Q06006.

Bucholz, C.E., Gaetani, G.A., and Behn, M.D. (2013) Post-entrapment modification of volatiles and oxygen fugacity in olivine-hosted melt inclusions: Earth and Planetary Science Letters, 374, 145–155.

Bureau, H., Raepsaet, C., Khodja, H., Carraro, A., and Aubaud, C. (2009) Determination of hydrogen content in geological samples using elastic recoil detection analysis (ERDA). Geochimica et Cosmochimica Acta, 73, 3311–3322.

Cabral, R.A., Jackson, M.G., Koga, K.T., Rose-Koga, E.F., Hauri, E.H., Whitehouse, M.J., Price, A.A., Day, J.M.D., Shimizu, N., and Kelley, K.A. (2014) Volatile cycling of H_2O, CO_2, F, and Cl in the HIMU mantle: A new window provided by melt inclusions from oceanic hot spot lavas at Mangaia, Cook Islands. Geochemistry Geophysics Geosystems, 15, 4445–4467.

Cadoux, A., Iacono-Marziano, G., Paonita, A., Deloule, E., Aiuppa, A., Nelson Eby, G., Costa, M., Brusca, L., Berlo, K., Geraki, K., Mather, T.A., Pyle, D.M., and Di Carlo, I. (2017) A new set of standards for in – situ measurement of bromine abundances in natural silicate glasses: Application to SR-XRF, LA-ICP-MS and SIMS techniques. Chemical Geology, 452, 60–70.

Carroll M.K. and Rutherford M.J. (1988) Sulfur speciation in hydrous experimental glasses of varying oxidation state--results from measured wavelength shifts of sulfur X-rays. American Mineralogist, 73, 845-849.

Carroll M.K. and Webster J.D. (1994) Solubilities of sulfur, noble gases, nitrogen, chlorine, and fluorine in magmas. In Carroll M. and Holloway J. Eds., Volatiles in Magmas, 30, p. 231-279. Reviews in Mineralogy and Geochemistry, Mineralogical Society of America, Chantilly, Virginia.

Carvalho, B., Bartoli, O., Ferri, F., Cesare, B., Ferrero, S., Remusat, L., Capizzi, L.S., Poli, S. (2019) Anatexis and fluid regime of the deep continental crust: New clues from melt and fluid inclusions in metapelitic migmatites from Ivrea Zone (NW Italy). Journal of Metamorphic Geology, 37, 951-975.

Créon, L., Levresse, G., Remusat, L., Bureau, H., Carrasco-Núñez, G. (2018) New method for initial composition determination of crystallized silicate melt inclusions. Chemical Geology, 483, 162-173.

Créon, L., Rouchon, V., Youssef, S., Rosenberg, E., Delpech, G., Szabó, C., Remusat, L., Mostefaoui, S., Asimow, P.D., Antoshechkina, P.M., Ghiorso, M.S., Boller, E., Guyot, F. (2017) Highly CO_2-supersaturated melts in the Pannonian lithospheric mantle - A transient carbon reservoir? Lithos, 286-287, 519-533.

Dalou, C., Koga, K.T., Le Voyer, M., and Shimizu, N. (2014) Contrasting partition behavior of F and Cl during hydrous mantle melting: implications for Cl/F signature in arc magmas. Progress in Earth and Planetary Science, 1, 309.

Devine J.D., Sigurdsson H., and Davis A.N. (1984) Estimates of sulfur and chlorine yield to the atmosphere from volcanic eruptions and potential climatic effects. Journal of Geophysical Research, 89, 6309–6325.

Devine J.D., Gardner J.E., Brack,H.P., Layne G.D., Rutherford M.J. (1995) Comparison of microanalytical methods for estimating H_2O contents of silicic volcanic glasses. American Mineralogist, 80, 319–328.

Dixon J.E., Clague D.A. and Stolper E.M. (1991) Degassing history of water, sulfur, and carbon in submarine lavas from Kilauea volcano, Hawaii. Journal of Geology, 99, 371-394.

Döbeli, M., Kottler, C., Glaus, F., Suter, M. (2005) ERDA at the low energy limit. Nuclear Instruments and Methods in Physics Research, B 241, 428-435.

Embley, R.W., Jonasson, I.R., Perfit, M.R., Franklin, J.M., Tivey, M.A., Malahoff, A., Smith, M.F. and Francis, T.J.G. (1988) Submersible investigation of an extinct hydrothermal system on the Galapagos Ridge: Sulfide mound, stockwork zone, and differentiated lavas. Canadian Mineralogist, 26, 517-539.

Fialin, M., Wagner, C., Métrich, N., Humler, E., Galoisy, L., Bézos, A. (2001) $Fe3^{+}/\Sigma Fe$ versus Fe Lα peak energy for minerals and glasses: recent advances with the electron microprobe. American Mineralogist, 86, 456–465.

Fialin, M., Bézos, A., Wagner, C., Magnien, V., Humler, E. (2004) Quantitative electron microprobe analysis of $Fe3^{+}/\Sigma Fe$: basic concepts and experimental protocol for glasses. American Mineralogist, 89, 654–662.

Fischer, T.P. (2008) Fluxes of volatiles (H_2O, CO_2, N_2, Cl, F) from arc volcanoes. Geochemical Journal, 42, 21–38.

Gaetani, G.A., O'Leary, J.A., Shimizu, N., Bucholz, C.E., and Newville, M. (2012) Rapid reequilibration of H2O and oxygen fugacity in olivine-hosted melt inclusions. Geology, 40, 915–918.

Guggino, S.N. and Hervig, R.L. (2010) Determination of fluorine in fourteen microanalytical geologic reference materials using SIMS, EPMA and proton induced gamma ray emission (PIGE) analysis. American Geophysical Union, Fall Meeting 2010, V51C-2209.

Hanley, J.J. and Koga, K.T. (2018) Halogens in Terrestrial and Cosmic Geochemical Systems: Abundances, Geochemical Behaviors, and Analytical Methods. In D. E. Harlov and L. Aranovich Eds., The Role of Halogens in Terrestrial and Extraterrestrial Geochemical Processes, p. 21-121. Springer Geochemistry, Spinger International Publishing, Switzerland.

Harlov, D.E. and Aranovich, L. (2018) The Role of Halogens in Terrestrial and Extraterrestrial Geochemical Processes, 1030 p. Spinger International Publishing, Switzerland,.

Hauri, E., Wang, J., Dixon, J.E., King, P.L., Mandeville, C., Newman, S. (2002) SIMS analysis of volatiles in silicate glasses 1. Calibration, matrix effects and comparisons with FTIR. Chemical Geology, 183, 99– 114.

Helo, C., Longpré, M.-A., Shimizu, N., Clague, D.A., and Stix, J. (2011) Explosive eruptions at mid-ocean ridges driven by CO_2-rich magmas. Nature Geoscience, 4, 260–263.

Ihinger, P.D., Hervig, R.L. and McMillan, P.F. (1994) Analytical methods for volatiles in glasses. In Carroll M. and Holloway J. Eds., Volatiles in Magmas, 30, p. 67-121. Reviews in Mineralogy and Geochemistry, Mineralogical Society of America, Chantilly, Virginia.

Jackson, M.G., Cabral, R.A., Rose-Koga, E.F., Koga, K.T., Price, A., Hauri, E.H., and Michael, P. (2015) Ultra-depleted melts in olivine-hosted melt inclusions from the Ontong Java Plateau. Chemical Geology, 414, 124-137.

Jarosewich, E., Nelen, J.A., and Norberg, J.A. (1979) Electron microprobe reference samples for mineral analysis. In Fudali, R.F. Ed., Smithsonian Contributions to the Earth Sciences, 22, 68-72.

Jarosewich, E. (2002) Smithsonian Microbeam Standards. Journal of Research of the National Institute of Standards and Technology, 107, 681-685.

Jochum, K.P., Dingwell, D.B., Rocholl, A., Stoll, B., Hofmann, A.W., Becker, J.S., Besmehn, A., Bessette, D., Dietze, H.-J., Dulski, P., Erzinger, J., Hellebrand, E., Hoppe, P., Horn, I., Janssens, K., Jenner, G.A., Klein, M., McDonough, W.F., Maetz, M, Mezger, K., Münker, C., Nikogosian, I.K., Pickhardt, C., Raczek, I., Rhede, D., Seufert, H.M., Simakin, S.G., Sobolev, A.V., Spettel, B., Straub, S. M., Vincze, L., Wallianos, A., Weckwerth, G., Weyer, S., Wolf, D., Zimmer, M. (2000) The preparation and preliminary characterisation of eight geological MPI-DING reference glasses for in-situ microanalysis. Geostandards Newsletter: The Journal of Geostandards and Geoanalysis, 24, 87-133.

Jochum, K. P., Stoll B., Herwig K., Willbold M., Hofmann A.W. , Amini M., Aarburg S., Abouchami W., Hellebrand E., Mocek B., Raczek I., Stracke A., Alard O., Bouman C., Becker S., Ducking M., Bratz H., Klemd R., de Bruin D., Canil D., Cornell D., de Hoog CJ, Dalpe C., Danyushevsky L., Eisenhauer A., Gao Y., Snow J.E., Groschopf N., Gunther D., Latkoczy C., Guillong M., Hauri E.H., Hofer H.E., Lahaye, Horz K., Jacob D.E., Kasemann S.A., Kent A.J.K., Ludwig T., Zack T., Mason P.R.D., Meixner A., Rosner M., Misawa K., Nash B.P., Pfander J., Premo W.R., Sun W.D., Tiepolo M., Vannucci R., Vennemann T., Wayne D., Woodhead J.D. (2006) MPI-DING reference glasses for in situ microanalysis: New reference values for element concentrations and isotope ratios. Geochemistry Geophysics Geosystems, 7, Q02008.

King, P.L., and Holloway, J.R. (2002) CO_2 solubility and speciation in intermediate (andesitic) melts: the role of H_2O and composition. Geochimica et Cosmochimica Acta, 66, 1627–1640.

Koga, K.T., Hauri, E.H., Hirschmann, M.M., and Bell, D.R. (2003) Hydrogen concentration analyses using SIMS and FTIR: Comparison and calibration for nominally anhydrous minerals. Geochemistry Geophysics Geosystems, 4, Q1019.

Koga, K.T., and Rose-Koga, E.F. (2018) Fluorine. In White, W.M. Ed., Encyclopedia of Geochemistry, p. 495-498, Springer Ineternational Publishing, Switzerland.

Koga, K.T., and Rose-Koga, E.F. (2018) Fluorine in the Earth and the solar system, where does it come from and can it be found? Comptes Rendus Chimie, 21, 749–756.

Kottler, C., Döbeli, M., Glaus, F., Suter, M. (2006) A spectrometer for low energy heavy ion ERDA. Nuclear Instruments and Methodes in Physics Research B, 248, 155-162.

Le Voyer, M., Rose-Koga, E.F., Laubier, M. and Schiano, P. (2008) Petrogenesis of arc lavas from the Rucu Pichincha and Pan de Azucar volcanoes (Ecuadorian arc): Major, trace element, and boron isotope evidences from olivine-hosted melt inclusions. Geochemistry Geophysics Geosystemes, 9, Q12027.

Le Voyer, M., Rose-Koga, E.F., Shimizu, N., Grove, T.L. and Schiano, P. (2010) Two contrasting H_2O-rich components in primary melt inclusions from Mount Shasta, Journal of Petrology, 51, 1571-1595, doi:10.1093/petrology/egq030.

Le Voyer, M., Asimow, P.D., Mosenfelder, J.L., Guan, Y., Wallace, P.J., Schiano, P., Stolper, E.M., and Eiler, J.M. (2014) Zonation of H_2O and F Concentrations around melt inclusions in olivines. Journal of Petrology, 55, 685–707.

Le Voyer, M., Kelley, K.A., Cottrell, E. and Hauri, E.H. (2017) Heterogeneity in mantle carbon content from CO_2-undersaturated basalts. Nature Communications, 8, 14062.

Le Voyer, M., Hauri, E.H., Cottrell, E., Kelley, K.A., Salters, V.J.M., Langmuir, C.H., Hilton, D.R., Barry, P.H., and Füri, E. (2019) Carbon fluxes and primary magma CO_2 contents along the global mid‐ocean ridge system. Geochemistry Geophysics Geosystems, 20, 1387–1424.

Lloyd, A.S., Ruprecht, P., Hauri, E.H., Rose, W., Gonnermann, H.M., and Plank, T. (2014) NanoSIMS results from olivine-hosted melt embayments: Magma ascent rate during explosive basaltic eruptions. Journal of Volcanology and Geothermal Research, 283, 1–18.

Métrich, N. and Rutherford, M.J. (1991) Experimental study of chlorine behavior in hydrous silicic melts. Geochimica et Cosmochimica Acta, 56, 607-616.

Métrich, N., Schiano, P., Clocchiatti, R., Maury, R.C. (1999) Transfer of sulfur in subduction settings: an example from Batan Island (Luzon volcanic arc, Philippines). Earth and Planetary Science Letters, 167, 1–14.

Métrich, N., and Wallace, P.J. (2008) Volatile abundances in basaltic magmas and their degassing paths tracked by melt inclusions. Reviews in Mineralogy and Geochemistry, 69, 363–402.

Michael, P.J., Cornell, W.C. (1998) Influence of spreading rate and magma supply on crystallization and assimilation beneath mid-ocean ridges: Evidence from chlorine and major element chemistry of mid-ocean ridge basalts. Journal of Geophysical Research-Solid Earth, 103, 18325-18356.

Mosbah, M., Métrich, N., Massiot, P. (1991) PIGME fluorine determination using a nuclear microprobe with application to glass inclusions. Nuclear Instruments and Methods in Physics Research B58, 227-231.

Narvaez, D.F., Rose-Koga, E.F., Samaniego, P., Koga, K.T., and Hidalgo, S. (2018) Constraining magma sources using primitive olivine-hosted melt inclusions from Puñali a and Sangay volcanoes (Ecuador). Contributions to Mineralogy and Petrology, 173, 79-104.

Oladottir, B., Sigmarsson O., Larsen G., and Devidal J-L. (2011) Provenance of basaltic tephra from Vatnajökull subglacial volcanoes, Iceland, as determined by major- and trace-element analyses. Holocene, 21, 1037–1048.

Oskarsson, N., Sigvaldason, G., Steinthorsson, S. (1982) A dynamic model of rift zone petrogenesis and the regional petrology of Iceland. Journal of Petrology, 23, 28-74.

Ottolini, L., Camara, F., Hawthorne, F.C., and Stirling, J. (2002) SIMS matrix effects in the analysis of light elements in silicate minerals: Comparison with SREF and EMPA data, American Mineralogist, 87, 1477-1485.

Perfit, M.R., Ridley, W.I., and Jonasson, I.R. (1998) Geologic, petrologic, and geochemical relationships between magmatism and massive sulfide mineralization along the Eastern Galapagos Spreading Center. In Barry T. and Hannington M. Eds., Reviews in Economic Geology-Volcanic-Associated Massive Sulfide Deposits, Society of Economic Geolology, New Haven, Connecticut.

Robinson, B.W., Graham, J. (1992) Advances in electron microprobe trace-element analysis. Journal of Computer-Assisted Microscopy, 4, 263–265.

Rose-Koga, E.F., Koga, K., Schiano, P., and Le Voyer, M., (2012) Mantle source heterogeneity for South Tyrrhenian magmas revealed by Pb isotopes and halogen contents of olivine-hosted melt inclusions. Chemical Geology, 334, 266–279.

Rose-Koga, E.F., Koga, K.T., Hamada, M., Hélouis, T., Whitehouse, M.J., and Shimizu, N. (2014) Volatile (F and Cl) concentrations in Iwate olivine-hosted melt inclusions indicating low-temperature subduction. Earth, Planets and Space, 66, 81-93.

Rose-Koga, E.F., Koga, K.T., Moreira, M., Vlastélic, I., Jackson, M.G., Whitehouse, M.J., Shimizu, N., and Habib, N. (2017) Geochemical systematics of Pb isotopes, fluorine, and sulfur in melt inclusions from Sã Miguel, Azores. Chemical Geology, 458, 22-37.

Shimizu, K., Suzuki, K., Saitoh, M., Konno, U., Kawagucci, S., and Ueno, Y. (2015) Simultaneous determinations of fluorine, chlorine, and sulfur in rock samples by ion chromatography combined with pyrohydrolysis, Geochemical Journal, 49, 113-124.

Shimizu, K., Ushikubo, T., Hamada, M., Itoh, S., Higashi, Y., Takahashi, E., and Ito, M. (2017) H_2O, CO_2, F, S, Cl, and P_2O_5 analyses of silicate glasses using SIMS: Report of volatile standard glasses. Geochemical Journal, 51, 299–313.

Shimizu, N., Semet, M., and Allègre, C.J. (1978) Geochemical applications of quantitative ion-microprobe analysis. Geochimica et Cosmachimica Acta, 42, 1321–1334.

Shimizu, N., and Hart, S.R. (1982) Application of the ion microprobe to Geochemistry and Cosmochemistry. Annual Reviews in Earth and Planetary Science, 10, 483–526.

Shimizu, N. (1998) The geochemistry of olivine hosted melt inclusions in a famous basalt ALV519-4-1. Physic of the Earth and Planetary Interior, 107, 183–201.

Simons, K., Dixon, J.E., Schilling, J.G., Kingsley, R.H., Poreda, R.J. (2002) Volatiles in basaltic glasses from the Easter-Salas y Gomez Seamount chain and Easter microplate: implications for geochemical cycling of volatile elements. Geochemistry Geophysics Geosystems, 3, 1-29.

Sims, KWW, Goldstein, SJ, Blichert-Toft, J, Perfit, MR, Kelemen, P, Fornari, DJ, Michael, P, Murrell, MT, Hart, SR, DePaolo, DJ, Layne G, Ball, L, Jull M, Bender, J (2002) Chemical and isotopic constraints on the generation and transport of magma beneath the East Pacific Rise. Geochimica et Cosmochimica Acta, 66, 3481-3504.

Sisson, T.W. and Layne, G.D. (1993) H_20 in basalt and basaltic andesite glass inclusions from four subduction-related volcanoes H_20 in basalt and basaltic andesite glass inclusions from four subduction-related volcanoes. Earth and Planetary Science Letters, 117, 619-635.

Straub, S.M. and Layne, G.D. (2003) The systematics of chlorine, fluorine, and water in Izu arc front volcanic rocks: Implications for volatile recycling in subduction zones. Geochimica et Cosmochimica Acta, 67, 4179-4203.

Stormer, JC, Pierson, ML,Tacker, RC (1993) Variation of F and Cl X-ray intensity due to anisotropic diffusion in apatite during electron microprobe analysi. American Mineralogist, 78, 641-648.

Thordarsson, T., Self, S., Oskarsson, N., Hulsebosch, T. (1996) Sulfur, chlorine, fluorine degassing and atmospheric loading by the 1783-1784 AD Laki (Skaftar Fires) eruption in Iceland. Bulletin of Volcanology, 58, 205-225.

Thornber, C. R., Sherrod D. R., Siems D. F., Heliker C. C., Meeker G. P., Oscarson R. L., and Kauahikaua J. P. (2002) Whole-rock and glass major-element chemistry of Kilauea Volcano, Hawaii, near-vent eruptive products: September 1994 through September 2001. U.S. Geol. Survey Open File Report, 02-17.

Todd, C.S. (1996) Fluorine analysis by electron microprobe: correction for iron interference. Abstract, GSA Annual Meeting, p.A-212. GSA, Boulder, Colorado.

Van den Bleeken, G., and Koga, K.T. (2015) Experimentally determined distribution of fluorine and chlorine upon hydrous slab melting, and implications for F–Cl cycling through subduction zones. Geochimica et Cosmochimica Acta, 171, 353–373.

Wade, J.A., Plank, T., Melson, W.G., Soto, G.J., Hauri, E.H. (2006) The volatile content of magmas from Arenal volcano, Costa Rica. Journal of Volcanology and Geothermal Research, 157, 94–120.

Wallace, P.J. (2005) Volatiles in subduction zone magmas: concentrations and fluxes based on melt inclusion and volcanic gas data. Journal of Volcanology and Geothermal Research, 140, 217-240.

Withers, A.C., Bureau, H., Raepsaet, C., and Hirschmann, M.M. (2012) Calibration of infrared spectroscopy by elastic recoil detection analysis of H in synthetic olivine. Chemical Geology, 334, 92–98.

Witter, J.B. and Kuehner, S.M. (2004) A simple empirical method for high-quality electron microprobe analysis of fluorine at trace levels in Fe-bearing minerals and glasses. American Mineralogist, 89, 57-63.

Zhang, C., Koepke, J., Wang, L.-X., Wolff, P.E., Wilke, S., Stechern, A., Almeev, R., and Holtz, F. (2016) A practical method for accurate measurement of trace level fluorine in mg- and fe-bearing minerals and glasses using electron probe microanalysis. Geostandards and Geoanalytical Research, 40, 351–363.

Figure caption

Fig. 1: Secondary ion spectra at nominal masses, 19 (a), 32 (b) and 35 (c) for a basalt glass (ALV519-4-1) to illustrate the resolution of isobaric interferences at M/ΔM=5800 (10% definition). This basalt glass contains 90 $\mu g.g^{-1}$ F, 950 $\mu g.g^{-1}$ S, and 45 $\mu g.g^{-1}$ Cl (Helo et al., 2011; Table 1).

Fig. 2: SIMS calibration curves for abundances of (a) fluorine, (b) chlorine, (c) sulfur in basalt glasses. The lines correspond to different fits. The red line is a weighted linear regression line forced through zero, and the blue line is a classic weighted linear regression line, the y-intercept giving the detection limit of the analyzed element. The gray field bounded by blue dashed lines indicates the 95% confience interval. The uncertainties of fitted coefficients represent one standard deviation. Reduced chi-square (χ_ν^2) values of fit are also reported. Since any of those fits are satisfactory within the error bars, we consider the calibrations to be linear over the range in S, Cl, F concentrations.

Fig. 3: Heavy Ion Elastic recoil detection analysis (HIERDA) spectra for oxygen ^{16}O (a), fluorine ^{19}F (b) and chloride ^{35}Cl (c). On the y-axis are reported the counts and on x-axis, the mass. This is the example of the measurements done on the standard MPI-DING glass KE12 (Jochum et al., 2006).

Fig. 4: concentrations of F (a), S (b) and Cl (c) measured by SIMS versus that measured by EPMA (circles) and HIERDA (square, when applies) on a log-log plot. Standards are categorized according to their SiO_2 contents into mafic, intermediate and acidic. The solid line is a one-to-one slope indicating perfect coherence of the fit.

Fig. 5: RSF (the relative sensitivity factor) is plotted against SiO_2 concentration in glass samples. RSF is determined for individual analysis of known samples. (a) RSF of fluorine, (b) of sulfur, and (c) of chlorine are shown here. There exists a slight negative slope for all the panels, however, due to scatter of measurements, the trend is not statistically significant. There are fewer RSF values for S because many of sulfur concentrations are below EPMA detection limit and there were no independent methods to verify their concentrations.

.

Table 1: F, S, Cl and SiO_2 measurements in 6 basalt glasses with the corresponding analytical methods and references. They are the glass-standards used for the calibration on the WHOI SIMS.

	F [ppm]	±	S [ppm]	±	Cl [ppm]	±	SiO_2 wt%	Mehod; Reference
ALV519-4-1	90	30	950	95	45	23	48.9	EPMA; [1]
ALV1654-3	997	150	1562	78	2914	146	56.7	EPMA; [1], [2]
ALV1649-3	445	67	1640	82	1433	72	51.5	EPMA; [1], [2]
GL03-D51-3	299	45	1126	57	182	18	49.5	EPMA; [1], [3]
GL07-D52-5	431	65	1183	59	322	32	48.6	EPMA; [1]
EN113-46D-2	124	37	877	88	45	23	49.5	EPMA; [1], [3]

[1] Helo et al., 2012; [2] Michael & Cornell, 1998; [3] Simons et al. 2002.
Relative analytical error for F concentration >200 ppm is 15% and F<200 ppm is 30%.
Relative analytical error for S concentration > 1000 ppm is 5% , between 100 to 1000 ppm is 10% and < 100 ppm is 50%.
Relative analytical error for Cl concentration >400 ppm is 5%, between 50 and 400 ppm is 10%, and Cl< 50 ppm is 50%.
Errors of these standards are assessed on the long term reproducibility.
SiO_2 was measured by EPMA

Table 2: Report of F, Cl, S and SiO_2 concentration measurements in 10 referenced material (*) and 3 other basaltic glasses (± is 2σ). Analytical methods and references are specified.

	F [ppm]	±	S [ppm]	±	Cl [ppm]	±	SiO_2 wt%	Method; Reference
ML3B-G*	70	18	1.2	0.12	7.5	1.4	51.4	SIMS [1]
			100	100	110	33		EPMA [1]
			30	30	60	18		EPMA [1]
	64;57;69	30;20;30						EPMA; SIMS; PIGE [2]
	71	**29**	**5.2**	**0.2**	**36**	**2**		**SIMS [WHOI this study]**
	63	20	7.0	1.0	55	6		SIMS [Eq. 6]
	48	*136*	*17*	*26*	*32*	*42*	**50.7**	**EPMA [LMV this study]**
StHs6/80-G*	320	32	2.7	0.3	184	18	63.7	SIMS [1]
			40	40	210	42		EPMA [1]
					230	69		EPMA [1]
	139;122;155	2;2;2						EPMA; SIMS; PIGE [2]
	n.d.		**4.3**	**0.2**	**27**	**1**		**SIMS; [WHOI this study]**
			6.0	0.6	48	2.5		SIMS [Eq. 6]
	28	*70*	*19*	*2*	*21*	*22*		**EPMA; [LMV this study]**
T1-G*	321	32	2.6	0.3	113	14	58.6	SIMS [1]
			30	30	100	50		EPMA [1]
					130	65		EPMA [1]
			0.92		119			LA-ICPMS [3]
			1.94					LA-ICPMS [3]
	107;94;119	6;6;8						EPMA, SIMS, PIGE [2]
	274	**79**	**6.0**	**0.2**	**175**	**15**		**SIMS [WHOI this study]**
	209	56	7.6	1.4	157	52		SIMS [Eq. 6]
	154	*47*	*20*	*8*	**158**	**7**	**57.5**	**EPMA [LMV this study]**
GOR128-G*	25	3	4.3	0.4	11.7	1	46.1	SIMS [1]
			30	30	50	35		EPMA [1]
					40	50		EPMA [1]
	n.d.		**8.3**	**0.4**	**38**	**2**		**SIMS [WHOI this study]**
			10	3	56	6		SIMS [Eq. 6]
	4	*16*	*15*	*20*	*38*	*37*	**45.5**	**EPMA [LMV this study]**
GOR132-G*	22	2	1.8	0.2	6.2	1	45.5	SIMS [1]
			50	50	30	30		EPMA [1]
					50	75		EPMA [1]
	n.d.		**5.7**	**0.2**	**30**	**1**		**SIMS [WHOI this study]**
			7.7	1.3	50	3		SIMS [Eq. 6]
	4	*16*	*11*	*26*	*24*	*34*	**44.3**	**EPMA [LMV this study]**
VG2*, *aka* USNM 111240/52	334	14					50.6	SIMS [4]
			1348	124	291	104		EPMA [5]
			1365	58	316	38		EPMA [5]
			1340	160				EPMA [6]
			1305	135				EPMA [7]
			1200	160	270	80		EPMA [8]
			1416	72	303	112		EPMA [9]

			1500					EPMA [10]
	243	**71**	**1440**	**110**	**325**	**30**		**SIMS [WHOI this study]**
	224	49	1350	740	263	99		SIMS [Eq. 6]
	210	*130*	**1343**	**46**	**306**	**26**		**EPMA [LMV this study]**
VG-A99*, aka A99, USNM 113498/1			170	60				EPMA [6]
			135	100	229	80		EPMA [5]
	765	158	220	48	227	40		EPMA [5]
			177	42	212	62		EPMA [9]
			96	63				EPMA [7]
			200	100				EPMA [11]
	709	47					51.1	SIMS [4]
	976	8						EPMA [12]
			175	116	205	60		EPMA [13]
	799	**208**	**141**	**10**	**220**	**19**		**SIMS [WHOI this study]**
	732	143	133	71	188	65		SIMS [Eq. 6]
	597	**98**	**130**	**22**	**210**	**20**		**EPMA [LMV this study]**
B6*					3300	200	75.3	EPMA [14]
Sletta	**3306**	**340**	*28*	*18*	**2075**	**64**		**EPMA [LMV this study]**
KL2-G*	177	28	7.7	1.3	22.4	4.5	50.3	SIMS [1]
			90	54	40	32		EPMA [1]
			320	320	60	18		EPMA [1]
	114;101;128	2;2;4						EPMA; SIMS; PIGE [2]
	114	**40**	**9.1**	**0.5**	**45**	**2**		**SIMS [WHOI this study]**
	105	27	10.7	3.0	61	8		SIMS [Eq. 6]
	99	*310*	*23*	*30*	**51**	**40**	**50.5**	**EPMA [LMV this study]**
	<71				*<324*			**ERDA [Zurich this study]**
ATHO-G*	770				530		74.5	EPMA [15]
	0.7	0.07	0.6	0.07	2430	0	75.6	SIMS [1]
			50	50	570	114		EPMA [1]
			200	140	510	102		EPMA [1]
	900	900	240	240	400	160		EPMA [1]
	1460	**370**	**4.8**	**0.2**	**680**	**64**		**SIMS [WHOI this study]**
	640	290	6.2	0.8	550	260		SIMS [Eq. 6]
	670	**400**	*17*	*24*	**453**	**44**	**74.1**	**EPMA [LMV this study]**
	637	**158**			**334**	**196**		**ERDA [Zurich this study]**
KE12*	4338	1096						EPMA [16]
	4400							EPMA [16]
					3270	110	70.8	EPMA [17]
	4200				3300			EPMA [17]
	4000	240						Selective ion method [18]
					3225	160		EPMA [19]
					3200	800		EPMA [20]
	4513	88						EPMA [12]
	7540	**1860**	**290**	**22**	**4670**	**450**		**SIMS [WHOI this study]**
	3910	1430	210	150	3570	1640		SIMS [Eq. 6]
	4490	**300**	**150**	**28**	**3410**	**110**		**EPMA [LMV this study]**

	3848	**230**			**3483**	**400**		**ERDA [Zurich this study]**
Alvin 2390-5	**300**	**70**	**1270**	**18**	**358**	**10**	**49**	**EPMA [LMV this study]**
Alvin 2746-15	**123**	**4**	**1449**	**30**	**890**	**18**	**50**	**EPMA [LMV this study]**

[1] Jochum et al. 2006; [2] Guggino and Hervig, 2010; [3] Diaz et al. 2006; [4] Straub & Layne 2003; [5] Thordasson et al. 1996; [6] Dixon et al. 1991; [7] Thornber et al., 2002; [8] Coombs et al. 2004; [9] DeHoog et al. 2001; [10] Hall et al. 2006; [11] Fisk & Kelley 2002; [12] Witter & Kuehner, 2004; [13] Streck & Wacaster 2006; [14] Tonarini et al. 2003; [15] Oskarsson et al. 1982; [16] Palais and Sigurdsson, 1989; [17] Métrich & Rutherford, 1991; [18] Mosbah et al, 1991; [19] Marianelli et al. 1995; [20] Cioni et al. 1998

Table 3: Result of error weighted regression of Eq. 5, and Eq. 6

	ak/dk	±	bk/ck	±	β	±	χ_ν^2
F (Eq. 5)	660	100	-4	2	-46	17	0.55
F (Eq. 6)	18	2	-0.18	0.02	-44	17	0.53
S (Eq. 5)	218	15	9.03	0.03	-90	12	3.40
S (Eq. 6)	18	4	-0.10	0.09	-94	50	3.37
Cl (Eq. 5)	-120	150	14	3	42	5	0.87
Cl (Eq. 6)	10	3	0.03	0.05	43	5	0.87

χ_ν^2 is a reduced chi-square statistics in which derived by a sum of square of difference between observation and prediction normalized by variance, then divided by the number of degree of freedom (*i.e.* the number of data minus 2).

This is a preprint, the final version is subject to change, of the American Mineralogist (MSA)
Cite as Authors (Year) Title. American Mineralogist, in press.
DOI: https://doi.org/10.2138/am-2020-7221

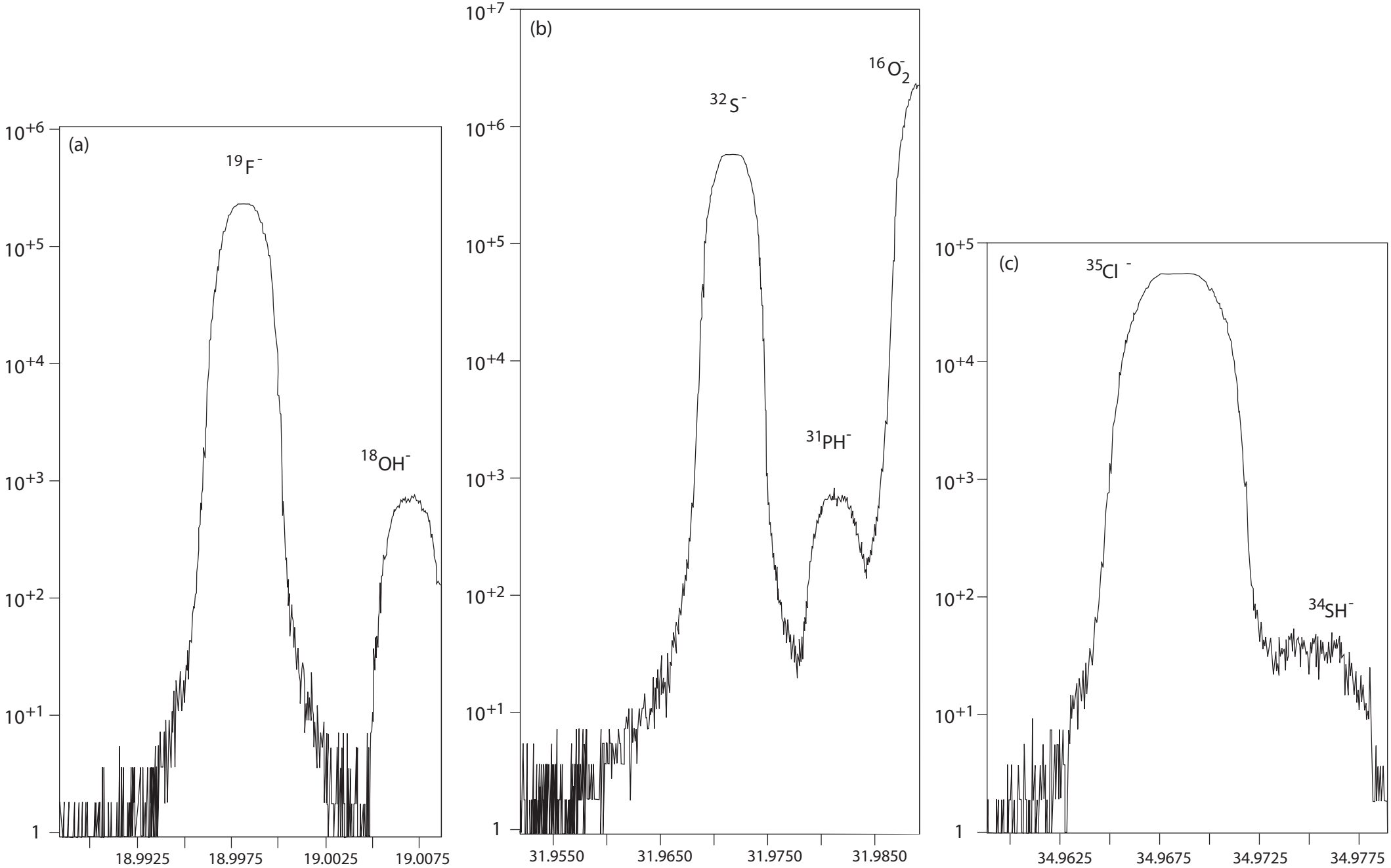

Fig. 1

This is a preprint, the final version is subject to change, of the American Mineralogist (MSA)
Cite as Authors (Year) Title. American Mineralogist, in press.
DOI: https://doi.org/10.2138/am-2020-7221

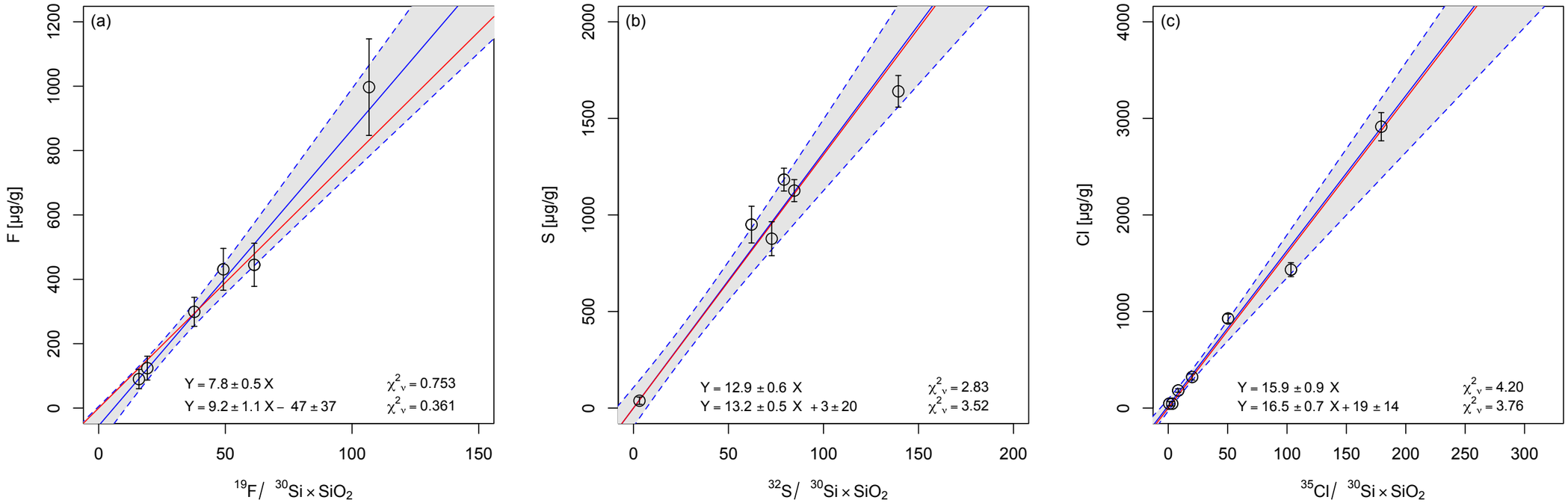

This is a preprint, the final version is subject to change, of the American Mineralogist (MSA)
Cite as Authors (Year) Title. American Mineralogist, in press.
DOI: https://doi.org/10.2138/am-2020-7221

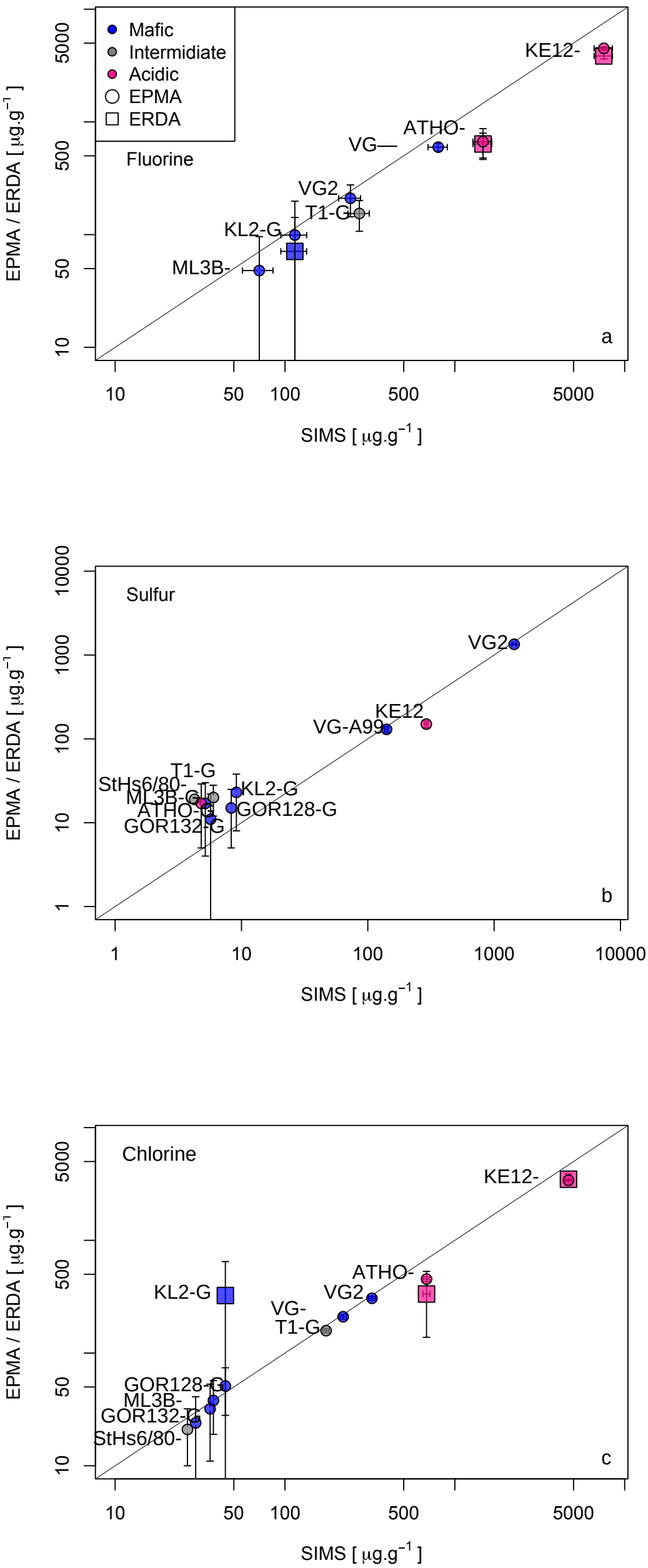

Fig. 4

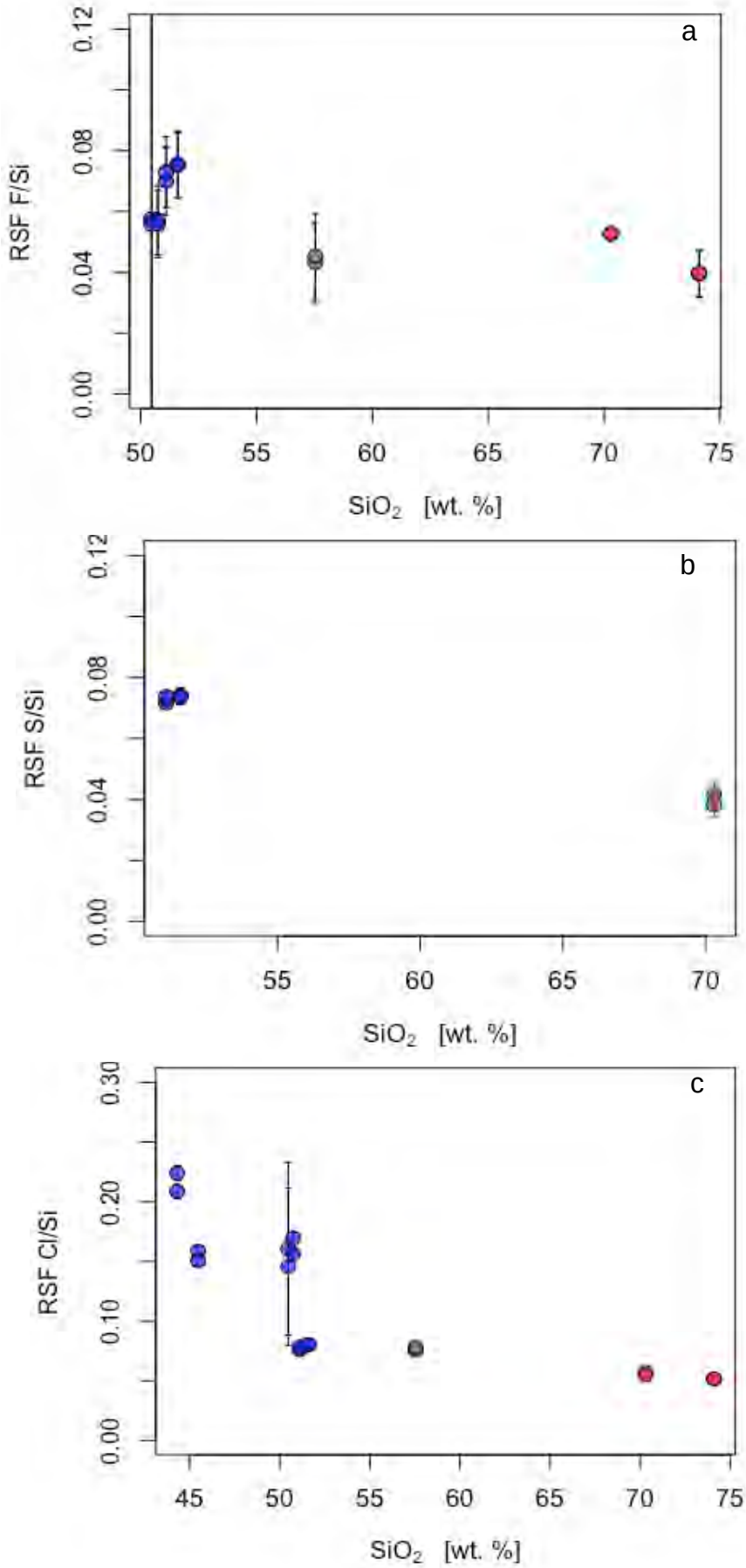
a
RSF F/Si
0.00
0.04
0.08
0.12
50
55
60
65
70
75
SiO2 [wt. %]
b
RSF S/Si
0.00
0.04
0.08
0.12
55
60
65
70
SiO2 [wt. %]
c
RSF Cl/Si
0.00
0.10
0.20
0.30
45
50
55
60
65
70
75
SiO2 [wt. %]

Fig. 5

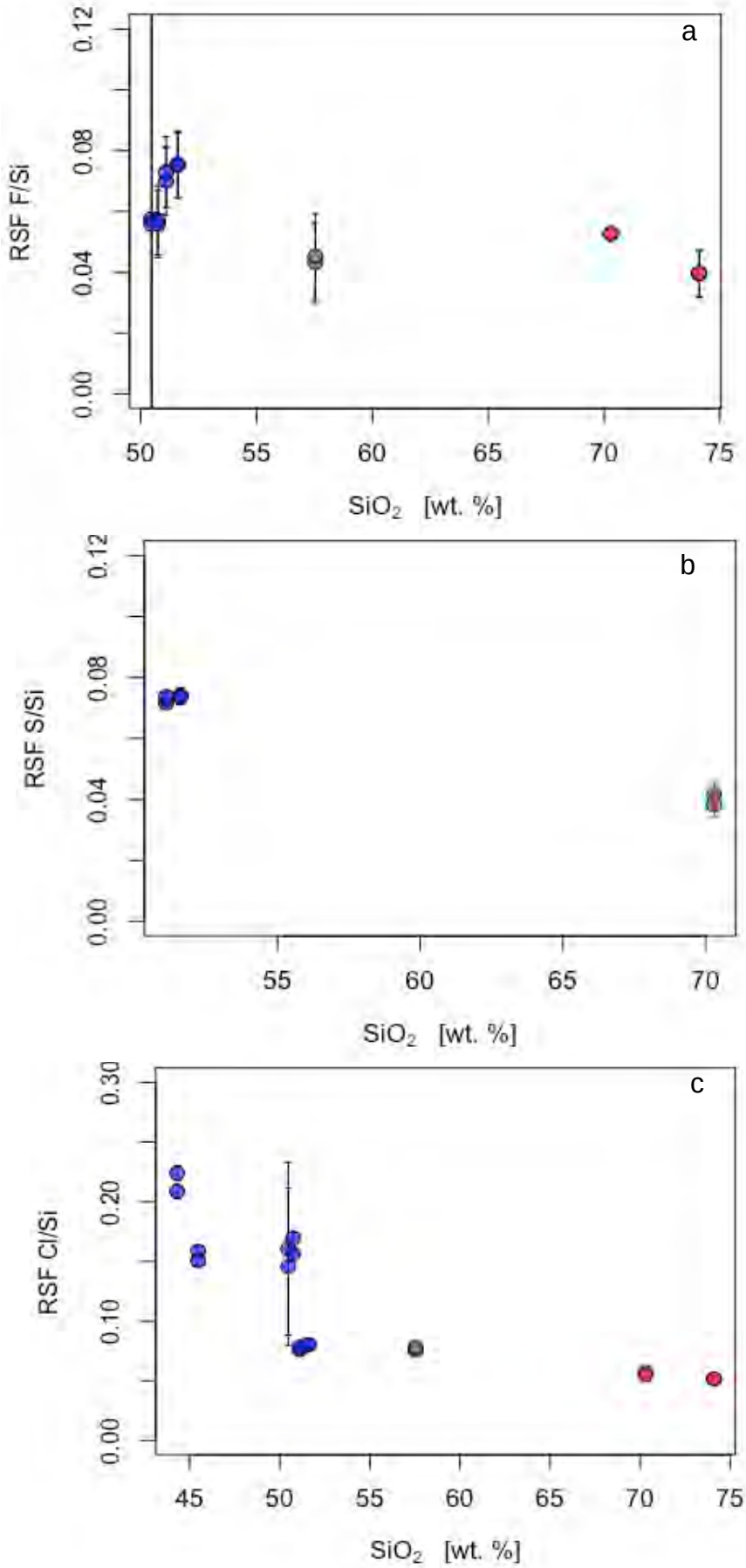
a
RSF F/Si
0.00
0.04
0.08
0.12
50
55
60
65
70
75
SiO2 [wt. %]
b
RSF S/Si
0.00
0.04
0.08
0.12
55
60
65
70
SiO2 [wt. %]
c
RSF Cl/Si
0.00
0.10
0.20
0.30
45
50
55
60
65
70
75
SiO2 [wt. %]

Fig. 5

This is a preprint, the final version is subject to change, of the American Mineralogist (MSA)
Cite as Authors (Year) Title. American Mineralogist, in press.
DOI: https://doi.org/10.2138/am-2020-7221

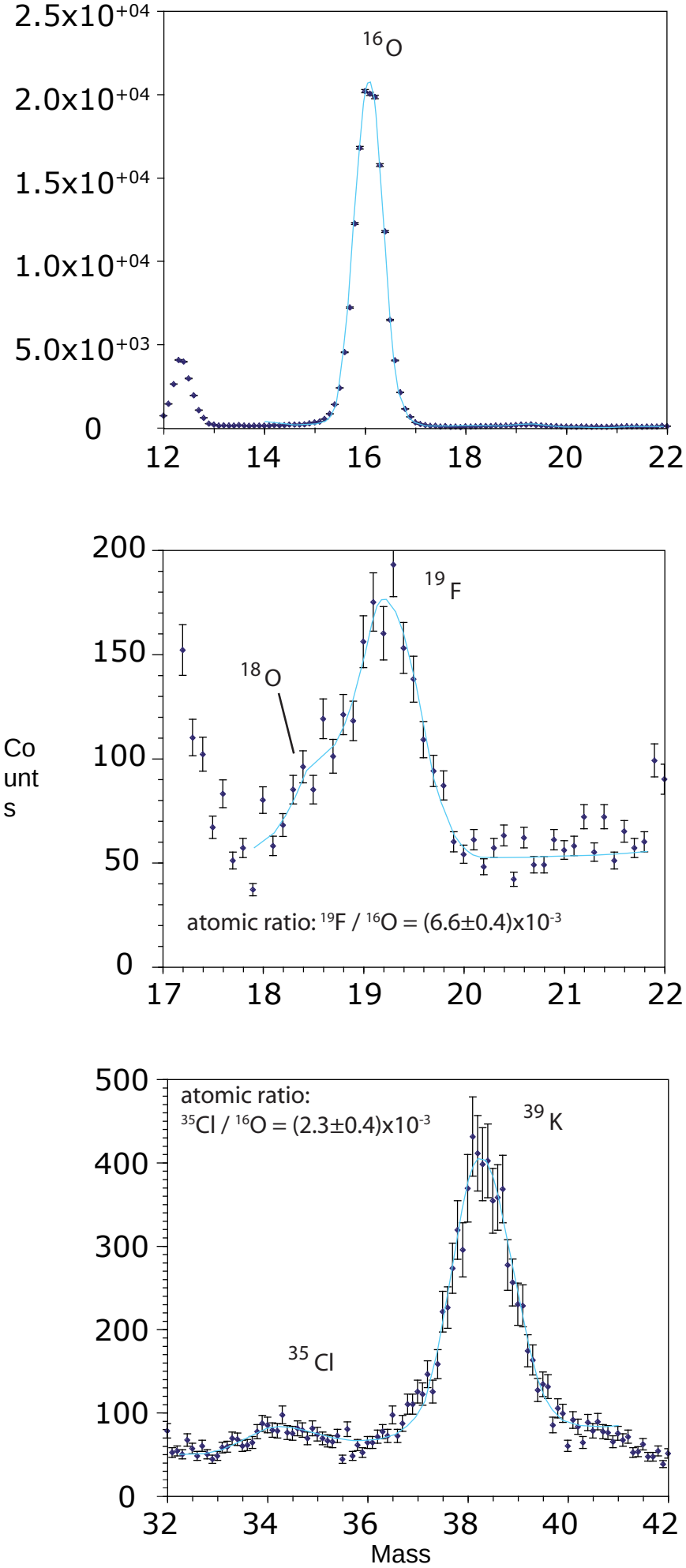

Fig. 3